Biotechnol Lett (2011) 33:1309–1317
DOI 10.1007/s10529-011-0587-7

ORIGINAL RESEARCH PAPER

A model of BmK CT in inhibiting glioma cell migration via matrix metalloproteinase-2 from experimental and molecular dynamics simulation study

Yue-Jun Fu · Na An · Kok-Gan Chan · Yan-Bo Wu · Shu-Hua Zheng · Ai-Hua Liang

Received: 18 January 2011 / Accepted: 4 March 2011 / Published online: 19 March 2011

Abstract The significance of BmK CT, a key chlorotoxin-like peptide isolated from the scorpion venom of *Buthus martensii* Karsch, is a novel blocker of the chloride ion channel and matrix metalloproteinase-2 (MMP-2). Site-directed mutagenesis of BmK CT, wound healing assay, gelatin zymography assay and computational simulation highlight the importance of electrostatic contribution to BmK CT–MMP-2 catalytic domain complex and a model of BmK CT–MMP-2 catalytic domain complex is therefore proposed. This is the first documentation of the structural mechanism of in the inhibition of glioma cell migration by BmK CT and may lead to the molecular design of specific inhibitors of MMP-2.

Y.-J. Fu (✉) · N. An · S.-H. Zheng · A.-H. Liang
Key Laboratory of Chemical Biology and Molecular Engineering of Ministry of Education, Institute of Biotechnology, Shanxi University, Taiyuan 030006, People's Republic of China
e-mail: yjfu@sxu.edu.cn

K.-G. Chan
Institute of Biological Sciences, Division of Genetics and Molecular Biology, Faculty of Science, University of Malaya, 50603 Kuala Lumpur, Malaysia

Y.-B. Wu
Key Laboratory of Chemical Biology and Molecular Engineering of Ministry of Education, Institute of Molecular Science, Shanxi University, Taiyuan 030006, People's Republic of China

Keywords BmK CT · Glioma cells · Matrix metalloproteinase-2 · Docking simulation

Introduction

Chinese scorpion *Buthus martensii* Karsch (BmK) venom is rich source of neurotoxins which bind to various ion channels with high affinity and specificity and are thus widely used as compounds to modulate signal transduction and channel gating (Chen et al. 2005). The first chlorotoxin (Cltx)-like peptide, BmK CT, isolated from the venom gland of *B. martensii* Karsch (Zeng et al. 2000), is a 36 mer peptide which is cross-linked by four disulfide bridges. Its sequence identity is 68% similar to Cltx isolated the scorpion *Leiurus quinquestriatus* (DeBin et al. 1993). Cltx binds specifically to glioma cell surface as a specific chloride channel blocker (Olsen et al. 2003). Preclinical studies suggest that ^{131}I-TM-601 (synthetic Cltx) might be an effective targeted therapy for the treatment of glioma (Mamelak et al. 2006). Our recent data indicate that BmK CT also shows specific toxicity against glioma cells but not astrocytes (Fu et al. 2007).

Gliomas can diffuse into the normal brain and this invasion of glioma cells involves modification of receptor-mediated adhesive properties of tumor cells, degradation, and remodeling of extracellular matrix by tumor-secreted metalloproteinases (MMPs) such as MMP-2, consequently creating an intercellular

space for invasion of glioma cells. MMP-2 activity is essential for invasion of glioma cells and Cltx inhibits invasion of glioma cells by modulating the surface expression of enzymatically active MMP-2 (Deshane et al. 2003).

Electrostatic effects play a pivotal role in the interaction between the ion channels and the small basic peptides of the scorpion toxins (Wu et al. 2004). In the present study, influence of basic residues in BmK CT on the inhibitory activity to MMP-2 was studied using computational methods and we now propose a model of the structural mechanism that may explain the inhibitory effect of this Cltx-like neurotoxin on glioma migration.

Materials and methods

Materials

DMEM was purchased from Gibco Life Technologies (NY, USA). Fetal calf serum (FCS) was purchased from the Institute of Hematology (Hang Zhou, China). Site-directed mutagenesis kit (TaKaRa MutanBEST Kit) was purchased from TaKaRa Biotechnology Co., Ltd (Dalian, China). Ni^{2+}-NTA agarose was obtained from Qiagen (Germany). Gelatin was purchased from Sigma. BmK CT encoding the Cltx-like peptide from the scorpion *B. martensii* Karsch was cloned according to the sequence optimized for codon usage in *Escherichia coli* and the expression plasmid pRSET C-BmK CT was constructed in our laboratory.

Prediction of three dimensional structure of protein by Swiss-Model workspace (http://swissmodel.expasy.org/) was performed as reported previously (Peitsch 1995; Guex and Peitsch 1997; Schwede et al. 2003; Kopp and Schwede 2004; Arnold et al. 2006). Protein–protein interactions by docking methods using ZDOCK (a fourier transform-based protein docking program) (http://zdock.bu.edu/) is preferred when high-resolution three dimensional structure of protein complex is not available (Wu et al. 2004). The quality of generated binding model is then further optimized by energy minimization and molecular dynamics (MD) simulation using Insight II 2000 software package developed by Accelrys.

Site-directed mutagenesis, expression, purification, and western blot analysis of BmK CT

Because BmK CT and Cltx are similar in primary structure, it is predicted that BmK CT may be functionally related to Cltx (Zeng et al. 2000). To analyze the location and function relationship of strong basic amino acid residues, K and R were mutated to a hydrophobic amino acid A (Table 1). Four different mutants were produced by PCR method using pRSET C-BmK CT as template.

Recombinant *E. coli* BL21 (DE3) cells were grown in LB medium supplemented with ampicillin (60 μg/ml) and incubated with shaking at 37°C. When the OD_{600} reached 0.6–0.7, the culture was induced with IPTG at 0.5 mM and shaken at 16°C for 8 h. Cells were harvested at 6,000×*g* for 30 min at 4°C, and then ultrasonicated. Cell debris was removed at 15,000×*g* for 30 min at 4°C. The supernatant was loaded onto a Ni^{2+}-NTA affinity column pre-equilibrated with buffer I (20 mM Tris/HCl buffer containing 10 mM imidazole and 500 mM NaCl, pH 9.0). The recombinant fusion protein of the bound His_6-tagged at the *N*-terminal was eluted with buffer II (20 mM Tris/HCl buffer containing 300 mM imidazole and 500 mM NaCl, pH 9.0). The eluent fraction containing BmK CT was collected, concentrated and desalted with 20 mM phosphate buffer (pH 7.4) at 4°C.

Table 1 Amino acid sequences of BmK CT and mutants

Name	Mutant residue(s)	Amino acid sequence
BmK CT	–	MCGPCFTTDANMA*RK*C*R*ECCGGIG*K*CFGPQCLCN*R*I
BmK $CT^{R14K15AA}$	R^{14}, K^{15}	MCGPCFTTDANMA*AA*CRECCGGIGKCFGPQCLCNRI
BmK CT^{R17A}	R^{17}	MCGPCFTTDANMARKC*A*ECCGGIGKCFGPQCLCNRI
BmK CT^{K25A}	K^{25}	MCGPCFTTDANMARKCRECCGGIG*A*CFGPQCLCNRI
BmK CT^{R35A}	R^{35}	MCGPCFTTDANMARKCRECCGGIGKCFGPQCLCN*A*I

Italics indicate the basic amino acid residues (R and K) that were separately mutated to the hydrophobic amino acid, A

Not all of the mutants could not be attached to the Ni^{2+}-NTA affinity column during the purification putatively due to the change of protein structure. Therefore, denaturation and refolding of mutants were performed. Briefly, IPTG-induced cells were harvested, followed by ultrasonication, and urea was added slowly to the total proteins to give 6 M. Debris was removed by centrifugation at 15,000×*g* for 25 min at 4°C and supernatant was loaded onto the Ni^{2+}-NTA affinity column and thoroughly washed with buffer I. His_6-tagged fusion mutant was eluted with buffer II. During the refolding process, urea was diluted gradually to 4, 2, 1, and 0.5 M. The resulting mutants were concentrated and desalted, respectively.

For western blot analysis, membrane was probed with the anti-His_6 tag mouse monoclonal antibody as the first antibody, followed by peroxidase-conjugated goat anti-mouse IgG (H+L) was used as the second antibody. Bound antibody was detected using an ECL Enhanced Chemiluminescence Detection Kit.

Circular dichroism (CD) analysis

The CD spectra of BmK CT and mutants were collected using Bio-Logic MOS-450 spectropolarimeter (France), with protein concentration of 0.4 mg/ml suspended in PBS buffer. Spectra were measured over the wavelength range from 200 to 240 nm at room temperature. CD spectra data obtained were average of three scans.

In vitro wound healing assay

The effect of BmK CT and mutants on cell migration was examined using in vitro wound healing assay. C6 cells were grown to a confluent monolayer in 96 multiwell microtiter plates. The "scratch" was introduced by scraping the C6 cells monolayer with a p200 pipette tip and was then washed three times with cell culture medium to remove cell debris. BmK CT was initially diluted in PBS and then serially diluted (0.15, 0.30, 0.6, 1.2, and 2.4 μM) in cell culture medium. BmK CT and mutants were diluted in cell culture medium to 0.15 μM which was identified as an appropriate concentration for detection of cell migration inhibition. Percent inhibition rate (IR%) was calculated according to the following equation: $IR\% = (1 - T/C) \times 100\%$, where T and C represent the mean migration distance of the treated group and the control group, respectively.

Gelatin zymography assay

Gelatinolytic activity of MMP-2 was analyzed by gelatin zymography. The cell culture media were changed to serum-free cell culture media when C6 cells were grown to a confluent monolayer. Then, BmK CT and mutants were diluted in these serum-free cell culture media to 0.15 μM. Serum-free media conditioned for 48 h were subjected to SDS-PAGE using 10% (v/v) gels containing 0.1% gelatin. The gel was incubated twice (for 30 min at room temperature) in 2.5% Triton X-100. The gel was incubated in activation buffer (5 mM $CaCl_2$, 1 μM $ZnCl_2$, and 0.005% Brij, 50 mM Tris/HCl, pH 8.0) overnight at 37°C. Gel was then stained with Coomassie Brilliant Blue R-250 and briefly destained in 10% (v/v) acetic acid and 40% (v.v) methanol (Deshane et al. 2003; Lu et al. 2004). Gelatinolytic activity of MMP-2 was detected as a transparent band on the blue background.

Three dimensional structure simulation

To analyze the location and function relationship of basic amino acid residues, computational methods were used to simulate BmK CT (wild type and mutants) and catalytic domain of MMP-2 complexes. The atomic coordinates of Cltx (Protein Data Bank code: 1CHL), catalytic domain of MMP-2 or gelatinase A (R^{88}-P^{250}, PDB code: 1QIB) were obtained from the Protein Data Bank (Berman et al. 2000).

The structure of Cltx in solution has been determined using 2D ^1H NMR spectroscopy as reported previously (Lippens et al. 1995). The homologous spatial structure of BmK CT was modeled by using the solution structures of Cltx and insect toxin 15A (PDB code: 1SIS) from *Buthus erpeus* as templates through the Swiss-Model server. The atomic coordinates simulation of BmK $CT^{R14K15AA}$, BmK CT^{R17A}, BmK CT^{K25A}, and BmK CT^{R35A} was performed by Swiss-Model server.

Analysis of BmK CT–MMP-2 catalytic domain complex by ZDOCK and MD simulation

Prediction of BmK CT–MMP-2 catalytic domain complex was performed using ZDOCK which can

operate on a Java platform (Pierce and Weng 2005; Wiehe et al. 2005; Pierce et al. 2007). The modeled three dimensional structures were subjected to refinement by optimization (steepest descent), 300 steps of conjugate gradient minimization within 10 Å water layer model at every step. MD simulation was performed to examine the quality of the model structure via 150 ps with the step size of 1 fs at 298 K. All simulations mentioned above were accomplished without any constraint under the consistent-valence force field (CVFF) in Discover 3 module of Insight II 2000 software package.

Results and discussion

Expression, purification and western blot analysis of BmK CT and mutants

The genes encoding BmK CT^{R14K15AA}, BmK CT^{R17A}, BmK CT^{K25A}, and BmK CT^{R35A} were amplified by PCR using pRSET C-BmK CT as template.

BmK CT and mutants (~4 kDa) were expressed in *E. coli* BL21 (DE3) under IPTG induction where both showed high level of expression (Fig. 1a), amounting to approximately 20% of the total cellular proteins. All the BmK CT and mutants were expressed in the soluble form present in the supernatant. The BmK CT but not the mutant proteins could effectively bind to Ni^{2+}-NTA affinity resin. Consequently, the denaturation and refolding treatments of mutants were performed and BmK CT was also treated in the same process as control. The purified mutant proteins showed two bands on the 16% Tricine/SDS/polyacrylamide gel (Fig. 1b). Furthermore, western blot analysis showed that protein with molecular mass of 15 kDa could be the tetramer of the recombinant mutants (Fig. 1c). The CD spectra of BmK CT and mutants showed that they belonged to $\alpha+\beta$ type protein according to the ellipticity values of 208 and 222 nm (Fig. 1d).

In vitro wound healing assay

As shown in Fig. 2a, incubation of C6 cells with BmK CT inhibited cell migration in a dose-dependent manner. Inhibition of C6 cell migration by BmK CT increased significantly from 0.15 to 2.4 μM. However, microscopic examination revealed that the inhibition of C6 cell migration in glioma spheroids by BmK CT (0.6 and 1.2 μM BmK CT) was associated with retraction of the long protrusions at the front of the invading C6 cells (data not shown). When BmK CT was applied into the C6 cell medium at 2.4 μM (final concentration) and incubated for 8 h, BmK CT inhibited the proliferation of C6 cells significantly. Consequently, 0.15 μM (for both BmK CT and mutants) was selected as appropriate to compare the inhibition rates of C6 cell migration. As shown in Fig. 2b, the average inhibition rates of BmK CT, BmK CT (denaturation and refolding), BmK CT^{K25A} and BmK CT^{R35A} were ranging from 17 to 26%, which was two-fold higher than that of BmK CT^{R14K15AA} and BmK CT^{R17A}.

Gelatin zymography assay

BmK CT and mutants showed inhibitory effect on MMP-2 activity as compared with the control (Fig. 2c). Gelatin zymography assay suggested that BmK CT and mutants could inhibit migration of glioma cells via MMP-2. The inhibitory capability of BmK CT^{R14K15AA} and BmK CT^{R17A} was weaker than that of BmK CT, BmK CT^{K25A}, and BmK CT^{R35A}.

Electrostatic potential and structure–function relationship assay

To investigate the possible role of electrostatics for the structure–function relationships, the electrostatic surfaces for both BmK CT (wild type and mutants) and catalytic domain of MMP-2 were calculated by using DeepView V.3.7 (Fig. 3).

The MMP-2 catalytic domain contains three α-helices and five β-sheets are arranged in a typical matrixin fold, and two zinc ions (PDB code: 1QIB) (Falconi et al. 2003). Electrostatic potential surface analysis showed that negative charge was mainly distributed over the MMP-2 catalytic domain (Fig. 3a).

Structural model showed that the folded structure of BmK CT consisted mainly of a small two-stranded antiparallel β-sheet packed against an α-helix, which is in agreement with those observed in the known three dimensional structures of other short toxins (Fig. 3b).

The calculated electrostatic potential surface around the BmK CT molecule was found to be mainly positive, suggesting that this clustering of positively charged residues and the strong positive field might

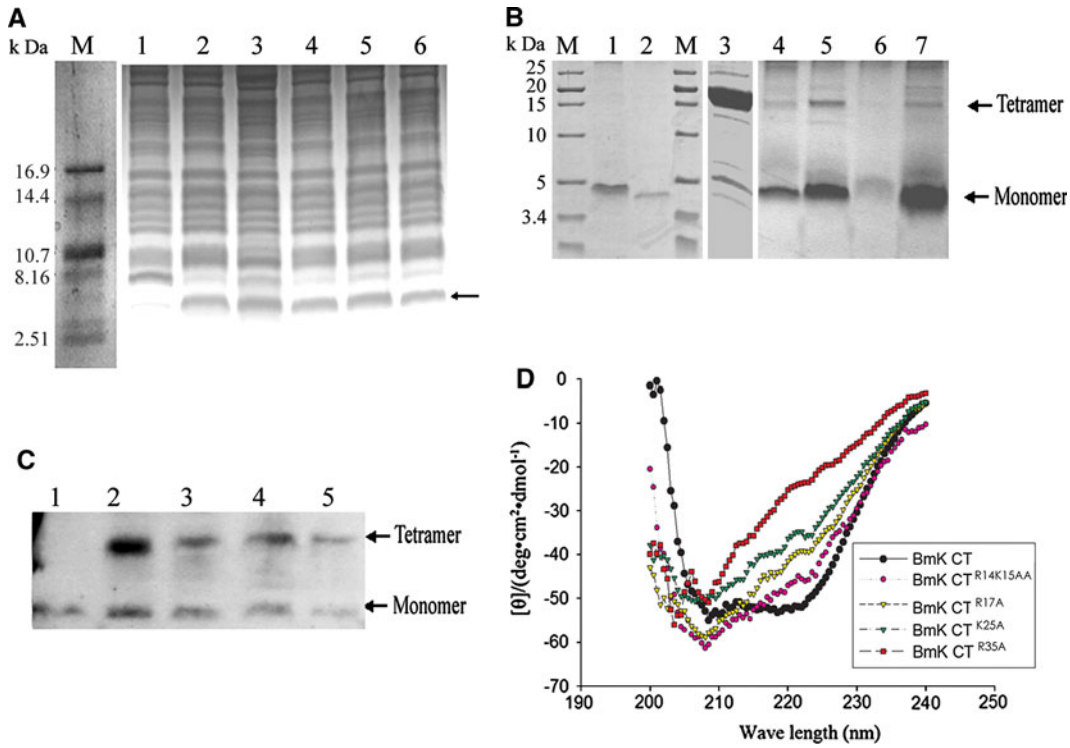

Fig. 1 **a** Expression of the His_6-taged BmK CT and mutants in *E. coli* BL21 (DE3) *M* low molecular weight markers proteins; *Lane 1* The total expressed protein of BL21 (DE3)/pRSET C; *Lanes 2–6* The total expressed proteins of BL21 (DE3)/pRSET C–BmK CT, BL21 (DE3)/pRSET C–BmK $CT^{R14K15AA}$, BL21 (DE3)/pRSET C–BmK CT^{R17A}, BL21 (DE3)/pRSET C–BmK CT^{K25A}, and BL21 (DE3)/pRSET C–BmK CT^{R35A}, respectively. The *arrow* shows the expression product His_6-taged BmK CT, BmK $CT^{R14K15AA}$, BmK CT^{R17A}, BmK CT^{K25A}, and BmK CT^{R35A} ($\sim$4 kDa). **b** Purification of BmK CT and mutants *Lanes 1*, *2* The purified target protein BmK CT washed with 300 mM imidazole without denaturation; *Lanes 3–7* The purified target proteins BmK CT, BmK $CT^{R14K15AA}$, BmK CT^{R17A}, BmK CT^{K25A}, and BmK CT^{R35A} with the treatments of denaturation, affinity chromatography, and refolding. The *arrows* indicated the monomer and tetramer of these target proteins, respectively. **c** Western blot analysis *Lanes 1–5* Western blot analysis of target proteins BmK CT, BmK $CT^{R14K15AA}$, BmK CT^{R17A}, BmK CT^{K25A}, and BmK CT^{R35A}, respectively. The tetramer of the mutants (15 kDa) is marked by *arrow* (upper position). **d** CD spectra

have important implications in the interaction with the receptor. The obvious change of electrostatic potential was accompanied by the mutation of $R^{14}K^{15}$ to $A^{14}A^{15}$ which was located in the beginning of α-helix, where it formed a neutral to negative zone (Fig. 3c). Obviously, as presented in the model of BmK $CT^{R14K15AA}$, the strong negatively charged zone rendered the positive surface in (or near) the α-helix disappeared completely, whereas the positive surface near the β-sheet was maintained by the positive residues. In Fig. 3d–f, strong polar charge was not formed by the mutation of one of the positive residues. These results showed clearly that strong electrostatic interaction existed between the interfaces in the BmK CT, mutants and MMP-2 catalytic domain. Also, it revealed that R^{14} and K^{15} of BmK CT played an important role of this interaction, which could affect the docking position or degree affinity.

Structural analysis of binding models between BmK CT (wild and mutant types) and MMP-2 catalytic domain complexes

The total energies of top ten ranked predictions are listed in Table 2. The lowest energy configurations were chosen for energy minimization and 150 ps MD simulation (Fig. 4). The electrostatic energies and interactive residues by hydrogen bond are shown in Table 3.

Two significant findings were presented in this work. Firstly, in structural aspect, based on the calculated electrostatic potential surface analysis, α-

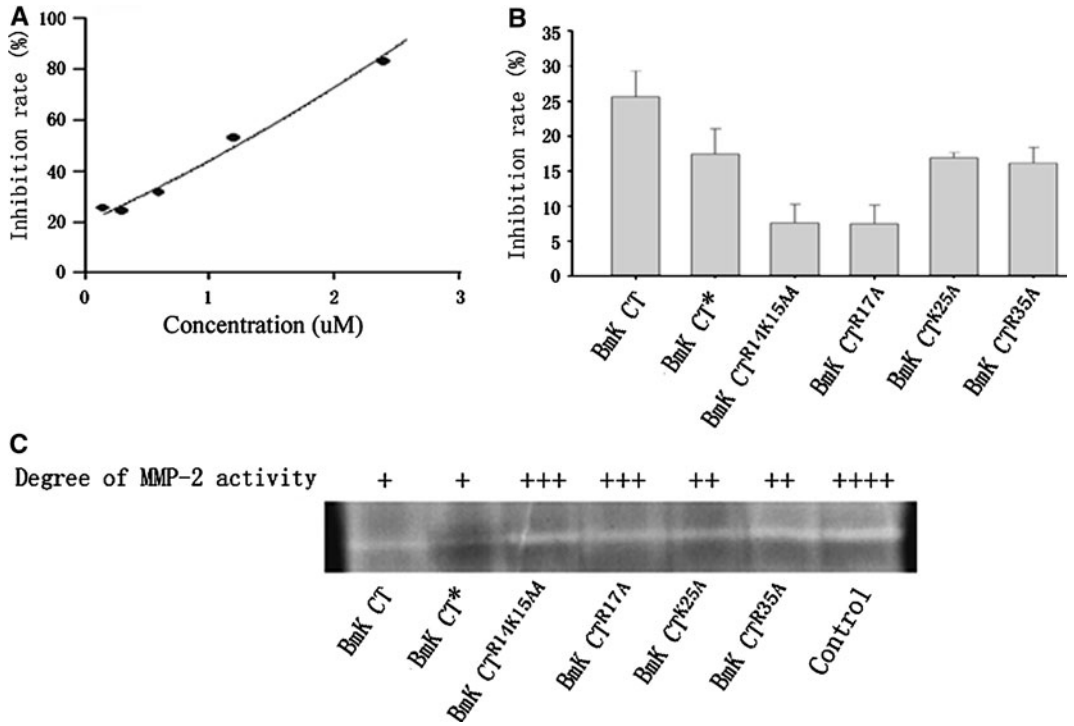

Fig. 2 BmK CT and mutants decreased C6 cell migration rate. **a** Migration of C6 cells was routinely monitored after confluent monolayers of C6 cells were gently scratched with a plastic pipette tip in the in vitro wound healing assay. The values of inhibition rate were regressed by SigmaPlot software. BmK CT inhibited the migration of glioma cells in a dose-dependent manner at the concentration ranging from 0.15 to 2.4 μM. **b** Inhibition rates of C6 cell migration were detected 8 h after treatment with BmK CT and mutants (0.15 μM). *BmK CT** denotes the BmK CT protein was treated by denaturation and refolding processes. **c** Gelatin zymography assay of MMP-2. BmK CT and mutants inhibited the catalytic activity of MMP-2. Degrees of MMP-2 activity were marked from "+ (minor)" to "++++ (significant)"

helices section of MMP-2 catalytic domain was the interactive interface bearing a large negative electrostatic potential for wild type and mutant BmK CT (Fig. 4). In Fig. 4a and Table 3, as for BmK CT, α-helix (R^{17}, C^{19}) was the only interface in the complex. As shown in Fig. 4b–e, the interfaces of BmK $CT^{R14K15AA}$, BmK CT^{R17A}, BmK CT^{K25A}, BmK CT^{R35A} were *β*-sheet 2 (Q30), *C*-terminal of α-helix (G21), α-helix (C19) and α-helix (R14), respectively, which suggested that α-helix was important for the location of BmK CT in the complexes. Once the mutation occurred in α-helix as demonstrated in BmK $CT^{R14K15AA}$ and BmK CT^{R17A}, the *β*-sheet 2 and C-terminal of α-helix were necessary in interacting with MMP-2 catalytic domain. So, three important basic residues namely $R^{14,17}$ and K^{15} were the active residues of BmK CT.

Secondly, with respect to the binding energy, electrostatic energy and the number of H_2 bonds are important for the tightness of the complex and can affect the functionality of BmK CT. The average values of total energies of BmK $CT^{R14K15AA}$–MMP-2 catalytic domain and BmK CT^{R17A}–MMP-2 catalytic domain complexes were 1531 and 1516 kcal/mol, respectively. These were higher than those of BmK CT–MMP-2 catalytic domain, BmK CT^{K25A}–MMP-2 catalytic domain and BmK CT^{R35A}–MMP-2 catalytic domain complexes. This result demonstrated that the structures of BmK CT–MMP-2 catalytic domain, BmK CT^{K25A}–MMP-2 catalytic domain and BmK CT^{R35A}–MMP-2 catalytic domain complexes were more stable than BmK $CT^{R14K15AA}$–MMP-2 catalytic domain and BmK CT^{R17A}–MMP-2 catalytic domain complexes. Moreover, according to the electrostatic energies and the number of interactive residues by hydrogen bond (Table 3), it was concluded that the structure of BmK CT–MMP-2 catalytic domain, BmK CT^{K25A}–MMP-2 catalytic domain and BmK

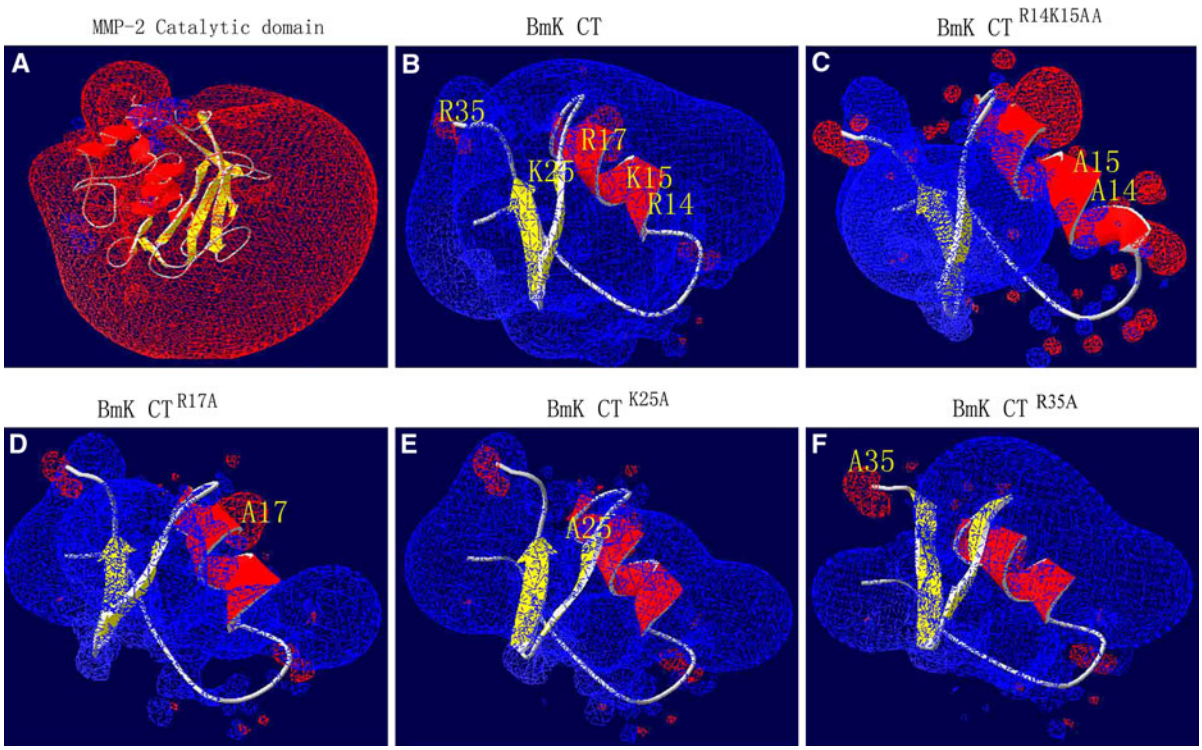

Fig. 3 Three dimensional structures and electrostatic surfaces of MMP-2 catalytic domain (**a**), BmK CT (**b**) and mutants (**c**–**f**) Electrostatic surfaces are calculated by the program DeepView V.3.7. Different color codes are −1.8 kT/e (*Red*) and 1.8 kT/e (*Blue*) where k is the Blotzmann constant, T is the temperature in Kelvin, and e is the charge of the electron. Positively charged residues are shown in *blue* and negatively charged in *red*. The basic amino acid residues of BmK CT and site-directed mutagenesis are shown in *yellow*

Table 2 Total energies of candidates of BmK CT and mutants–MMP-2 catalytic domain complexes

	1	2	3	4	5	6	7	8	9	10	Average
BmK CT–MMP-2 CD	1540	1309	1359	1582	1348	*1195*	1427	1417	1386	1403	1397
BmK $CT^{R14K15AA}$–MMP-2 CD	1438	1567	1464	1699	1509	1413	1716	*1388*	1592	1521	1531
BmK CT^{R17A}–MMP-2 CD	*1430*	1461	–	1496	1426	1563	1506	1765	1491	1506	1516
BmK CT^{K25A}–MMP-2 CD	1457	1414	1312	*1247*	1600	1438	1406	1449	–	1556	1431
BmK CT^{R35A}–MMP-2 CD	1444	1353	1359	1372	1311	*1305*	–	–	1347	1414	1363

All energies are in kcal/mol. MMP-2 CD: MMP-2 catalytic domain. "–" means the modles are not suitable for optimized in Biopolymer software. The values of all lowest energy configurations, which were chosen for energy minimization, molecular dynamics (MD) by Discover 3 and structural analysis, were *italicized*

CT^{R35A}–MMP-2 catalytic domain complex was tighter than that of BmK $CT^{R14K15AA}$–MMP-2 catalytic domain and BmK CT^{R17A}–MMP-2 catalytic domain complex. These factors led to the decrease of functionality of BmK $CT^{R14K15AA}$ and BmK CT^{R17A}.

Conclusion

In vitro experimental measurements and molecular dynamics simulation collectively showed that three important basic residues ($R^{14,17}$ and K^{15}) represented the active residues of BmK CT that interacted with

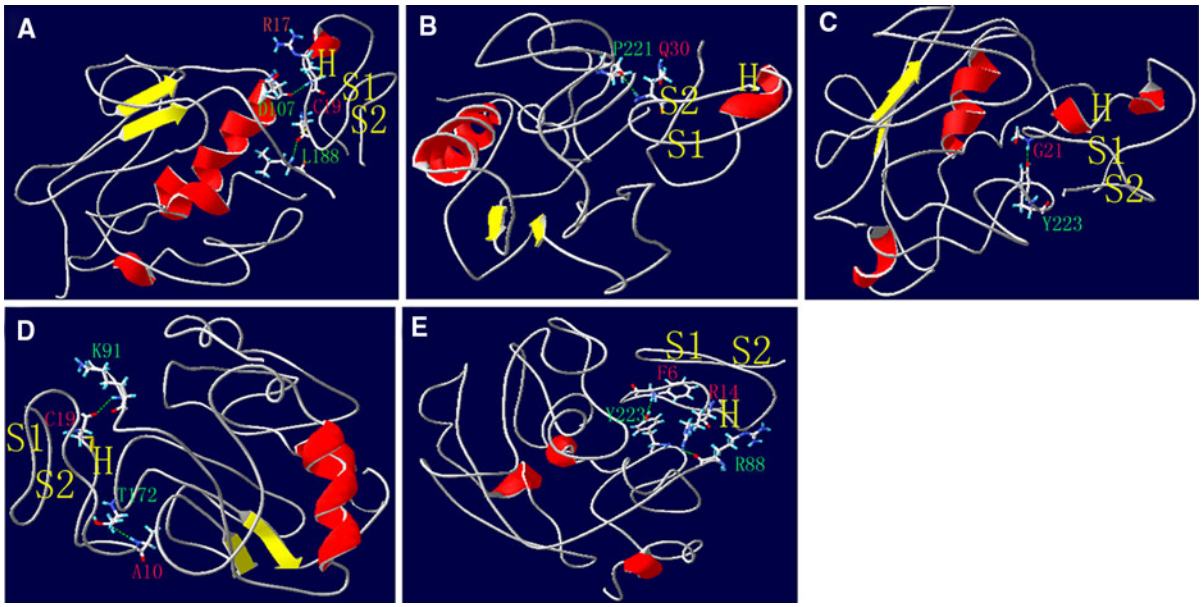

Fig. 4 Ribbon models of BmK CT–MMP-2 catalytic domain complex (**a**) and mutants–MMP-2 catalytic domain complexes (**b**–**e**) The whole backbones of complexes were shown. The α-helix (*H*) and β-sheets (*S1*, *S2*) in the BmK CT are explicitly labeled. The amino acid residues of contacts by hydrogen bond (indicated by *green line*) between BmK CT (or mutants) and MMP-2 catalytic domain were indicated

Table 3 Electrostatic energy and interactive residues by hydrogen bond of each minimum energy model

Minimum energy model	Electrostatic energy (kcal/mol)	Contacts between residue pairwise
BmK CT–MMP-2 CD (6)	−175.3	R17-D107 C19-L188
BmK CT^{R14K15AA}–MMP-2 CD (8)	−45.5	Q30-P221
BmK CT^{R17A}–MMP-2 CD (1)	−50.7	G21-Y223
BmK CT^{K25A}–MMP-2 CD (4)	−584.9	A10-T172 C19-K91
BmK CT^{R35A}–MMP-2 CD (6)	−241.6	F6-Y223 R14-R88

the catalytic domain of MMP-2. The study on structure and function of BmK CT may allow us to develop more inhibitive anti-MMP2 reagents against glioma cells.

Acknowledgments This project was supported by grants from "National Natural Science Foundation of China (No. 30700534)", "Natural Science Foundation of Shanxi Province (2008021039)" and "National High Technology Research and Development Program of China (863 Program)".

References

Arnold K, Bordoli L, Kopp J, Schwede T (2006) The SWISS-MODEL workspace: A web-based environment for protein structure homology modeling. Bioinformatics 22: 195–201

Berman HM, Westbrook J, Feng Z, Gilliland G, Bhat TN, Weissig H, Shindyalov IN, Bourne PE (2000) The protein data bank. Nucleic Acids Res 28:235–242

Chen X, Tong XT, Zhang NX, Wu G, Zhang Q, Wu HM (2005) Solution structure of BmP08, a novel short-chain scorpion toxin from *Buthus martensi* Karsch. Biochem Biophys Res Commun 330:1116–1126

DeBin JA, Maggio JE, Strichartz GR (1993) Purification and characterization of chlorotoxin, a chloride channel ligand from the venom of the scorpion. Am J Physiol 264:C361–C369

Deshane J, Garner CC, Sontheimer H (2003) Chlorotoxin inhibits glioma cell invasion via matrix metalloproteinase-2. J Biol Chem 278:4135–4144

Falconi M, Altobelli G, Iovino MC, Politi V, Desideri A (2003) Molecular dynamics simulation of matrix metalloproteinase 2: fluctuations and time evolution of recognition pockets. J Comput Aided Mol Des 17:837–848

Fu YJ, Yin LT, Liang AH, Zhang CF, Wang W, Chai BF, Yang JY, Fan XJ (2007) Therapeutic potential of chlorotoxin-like

neurotoxin from the Chinese scorpion for human gliomas. Neurosci Lett 412:62–67

Guex N, Peitsch MC (1997) SWISS-MODEL and the Swiss-PdbViewer: An environment for comparative protein modeling. Electrophoresis 18:2714–2723

Kopp J, Schwede T (2004) The SWISS-MODEL Repository of annotated three-dimensional protein structure homology models. Nucleic Acids Res 32:230–234

Lippens G, Najib J, Wodak SJ, Tartar A (1995) NMR sequential assignments and solution structure of chlorotoxin, a small scorpion toxin that blocks chloride channels. Biochemistry 34:13–21

Lu KV, Jong KA, Rajasekaran AK, Cloughesy TF, Mischel PS (2004) Upregulation of tissue inhibitor of metalloproteinases (TIMP)-2 promotes matrix metalloproteinase (MMP)-2 activation and cell invasion in a human glioblastoma cell line. Lab Invest 84:8–20

Mamelak AN, Rosenfeld S, Bucholz R, Raubitschek A, Nabors LB, Fiveash JB, Shen S, Khazaeli MB, Colcher D, Liu A, Osman M, Guthrie B, Schade-Bijur S, Hablitz DM, Alvarez VL, Gonda MA (2006) Phase I single-dose study of intracavitary-administered iodine-131-TM-601 in adults with recurrent high-grade glioma. J Clin Oncol 24: 3644–3650

Olsen ML, Schade S, Lyons SA, Amaral MD, Sontheimer H (2003) Expression of voltage-gated chloride channels in human glioma cells. J Neurosci 23:5572–5582

Peitsch MC (1995) Protein modeling by E-mail. Bio/Technology 13658–13660

Pierce B, Weng Z (2005) M-ZDOCK: A grid-based approach for Cn symmetric multimer docking. Bioinformatics 21:1472–1476

Pierce B, Phillips AT, Weng Z (2007) Computational methods for protein structure prediction and modeling: structure prediction. In: Xu Y, Xu D (eds) Structure prediction of protein complexes. Springer, New York, pp 109–134

Schwede T, Kopp J, Guex N, Peitsch MC (2003) SWISS-MODEL: an automated protein homology-modeling server. Nucleic Acids Res 31:3381–3385

Wiehe K, Pierce B, Mintseris J, Tong W, Anderson R, Chen R, Weng Z (2005) ZDOCK and RDOCK performance in CAPRI rounds 3, 4, and 5. Proteins 60:207–213

Wu YL, Cao ZJ, Yi H, Jiang DH, Mao X, Liu H, Li WX (2004) Simulation of the interaction between ScyTx and small conductance calcium-activated potassium channel by docking and MM-PBSA. Biophys J 87:105–112

Zeng XC, Li WX, Zhu SY, Peng F, Zhu ZH, Wu KL, Yang FH (2000) Cloning and characterization of a cDNA sequence encoding the precursor of a chlorotoxin-like peptide from the Chinese scorpion *Buthus martensii* Karsch. Toxicon 38:1009–1014